

NH₄-smectite: Characterization, hydration properties and hydro mechanical behaviour

M. Gautier^a, F. Muller^a, L. Le Forestier^a, J.-M. Beny^a and R. Guegan^a

^a Institut des Sciences de la Terre d'Orléans (ISTO), UMR 6113, Université d'Orléans, CNRS/INSU, Université François Rabelais, Tours, 1A rue de la Férollerie, 45071 Orléans Cedex 2, France

Abstract

Leachates in waste landfills are characterized by the presence of ammonium ions in large excess. These ammonium ions can be exchanged with the interlayer cations in clay and modify the physical and chemical properties of clay geochemical barriers in waste landfills and drive to environmental problems. The purpose of this study was to understand the hydro-physical changes of a smectite in the presence of ammonium ions. An ammonium smectite was prepared by cation exchange from a natural montmorillonite (Wyoming). The samples were characterized and their properties were compared by the use of a set of complementary techniques (X-ray diffraction, infrared spectroscopy, N₂ adsorption–desorption BET technique, thermal analysis, and percolation experiments). The main effect was a modification of the porosity and its network, and reduced crystalline swelling. These effects changed the hydraulic conductivity and macroscopic swelling of the clay. The oedometer experiments, which allow simulating the pressure on small amounts of samples, proved the strong increase of the permeability of NH₄-smectite. This last point is of great importance in an environment point of view and raises questions on the impermeability behaviour on the long term of the clay geochemical barriers with the presence of ammonium ions in waste landfills.

Keywords: Waste landfill; Clay geochemical barriers; Ammonium smectite; Hydraulic conductivity

1. Introduction

The percolation of water through waste landfills, together with the degradation of waste produces leachates with high amounts of pollutants. Generally, clay barriers are used in the bottoms of these sites to prevent any pollution in the soil and groundwater. Smectites are mainly selected due to their strong adsorption properties, their low permeability after compaction, their expansion ability, and their high cation exchange capacity (CEC).

The most important property of clay in the context of engineered barrier is impermeability (Jullien et al., 2002). The swelling of compacted clays has to prove its efficiency in terms of pollutant retention, but it must also respect the permeability requirements. In the case of waste landfills, clays come in contact with complex solutions, and the chemical composition of leachates can change the clay's macroscopic behaviour, especially its final hydraulic conductivity ([Daniel et al., 1993], [Shackelford, 1994], [Studds et al., 1996], [Coméaga, 1997], [Lin, 1998], [Alawaji, 1999], [Mohan et al., 1999], [Shackelford et al., 2000],

[Egloffstein, 2001] and [Jullien et al., 2002]). Due to waste mass, a clay barrier at the bottom of a waste landfill is under high pressure.

Landfill leachates are characterized by a high variety of cations, and among these, ammonium (NH_4^+) is one of the principal ones ([Belevi and Baccini, 1989], [Ehrig, 1989], [Robinson and Luo, 1991], [Dockhorn et al., 1997], [Christensen et al., 2001], [Baun and Christensen, 2004] and [Öman and Junestedt, 2008]), mainly produced by protein degradation processes. The NH_4^+ concentration gradually increases after the exploitation of waste landfills is over, due to the slow kinetic process of nitrogen mineralization reaching a maximum after several years. As a consequence, this compound can remain for hundreds of years as the major long-term pollutant source among inorganic compounds ([Kruempelbeck and Ehrig, 1999] and [Kjeldsen et al., 2002]). Öman and Junestedt (2008) also noted that despite the occasional presence of other nitrogen compounds in the leachate (nitrate, nitrite or organic nitrogen), the largest fraction of nitrogen is in the form of ammonium ions. Indeed, this assumption was supported by the study of Trabelsi et al. (2000) who showed that between 70 and 85% of total nitrogen in the leachate was present in the form of ammonium ions. Thus, the elimination of ammonium ions can only be performed by leaching, because no process of mineralization or oxidation (into NO_3^- or N_2) exists during methanogenesis.

In a clay barrier, ammonium can interact with clay by ion exchange and affect the texture and permeability of the resulting clay (Gaucher et al., 2006). The sequence of ion exchange selectivity by smectites described by (Stumm, 1992) and (McBride, 1994), then resumed by (Domenico and Schwartz, 1990) and (Malfoy, 2003) is as follows:

$\text{Al}^{3+} > \text{Ca}^{2+} > \text{Mg}^{2+} > \text{NH}_4^+ > \text{K}^+ > \text{Na}^+ > \text{Li}^+$. Among the monovalent cations, NH_4^+ is favoured, and a natural exchange with other monovalent cations in the interlayer space is easily possible. Since the bottoms of waste landfills are probably saturated with NH_4^+ cations, the exchange with the clay barrier will be facilitated. Pivato and Raga (2006) showed that the adsorption of ammonium in bentonites – compacted or not – was large, and advised the use of this clay type at the bottoms of waste landfills to limit ammonium pollution. Likewise, Guyonnet et al. (2005) showed that prehydrating the clay with a fluid seems to favour the access of NH_4^+ to exchange sites during leachate percolation.

The objectives of this study were first to characterize a NH_4 -smectite and then to understand the behaviour of this smectite in the specific context of waste landfills. Indeed, it may be helpful to consider the cation exchange between the initial cations (mainly calcium, sodium and potassium) in the clay barrier and ammonium ions. A complete description and characterization of percolation experiments under constant pressure in both compacted clays were performed to simulate the in-situ conditions of waste landfills and to evaluate the influence of the ammonium exchange on the main hydro-mechanical parameters: the hydraulic conductivity and the macroscopic swelling of the clays, which contribute to the final permeability value of the clay barrier.

2. Materials and methods

2.1. Materials

The smectite sample used for this study was the SWy-2 Wyoming montmorillonite supplied by the Source Clays Repository of Clay Minerals Society. The impurities identified as quartz, feldspar, gypsum, mica, and illite in the original smectite sample represented 5% after purification by $< 2 \mu\text{m}$ size separation (Chiperu and Bish, 2001). The structural formula of the

< 2 μm size fraction, calculated from the chemical composition given in Table 1, is



Approximately 2 g of the Wyoming montmorillonite were dispersed in 50 mL of a 1 M ammonium chloride solution. The sample was rotated on a SRT1 Stuart Scientific roller mixer for 12 h. The supernatant chloride solution was removed and replaced by a fresh 1 M NH_4Cl solution. This process was repeated five times. The sample was then introduced into a dialysis membrane tubing and placed in deionized water to remove the chloride ions. The water was changed daily until the chloride disappeared (AgNO_3 test). After dialysis and decantation, the < 2 μm size fraction of the NH_4 -smectite was separated, dried and finely hand ground in an agate mortar.

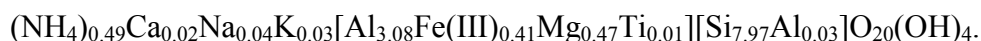
2.2. Sample characterizations

The chemical composition of the samples was determined by ICP-AES analysis using a Jobin-Yvon Ultima spectrometer. 100 mg of each sample was dissolved by alkaline fusion (LiBO_2) before the Si, Al, Fe, Ti, Mn, Mg, Li, Ca, Na, and K concentrations were measured.

Fourier Transform Infrared (FTIR) spectra were recorded using a NICOLET Magna-IR 760 Fourier transform spectrometer. To avoid the exchange with ions within the sample during the analysis (Pelletier et al., 1999), and to prohibit contributing absorbed water from KBr pellets, a NICOLET Nic-Plan microscope was used. The spectrometer and the microscope were purged with dry air to remove most of the atmospheric H_2O and CO_2 . The powder sample was spread over the NaCl window of the microscope stage. The analysed sample area was a 100 μm diameter circle chosen under the microscope 15 \times Cassegrainian objective. The operating conditions were 128 scans and 2 cm^{-1} resolution with no ambient CO_2 - H_2O corrections. The studied wave number range was 650–4000 cm^{-1} according to the spectrometer beam splitter and the microscope detector (NICOLET MCT-A). The analyses were performed in transmission mode.

The ammonium content was calculated from total nitrogen contents, which were determined by combustion of 40 mg of sample at 1573 K using an elemental analyser CNS 2000 LECO. The combustion process converted ammonium into N_2 and quantified by conductivity measurements.

With a set of 16 measurements, we determined \bar{N} , the mean value of the nitrogen content in ammonium smectites, and $\Delta\bar{N}$, the precision: $\bar{N} = 8.8 \text{ mg g}^{-1}$ with $\Delta\bar{N} = \pm 0.8 \text{ mg g}^{-1}$ (Gautier et al., 2009). This led to the structural formula of the exchanged NH_4 -smectite sample:



X-ray diffraction (XRD) patterns were recorded using a Thermo Electron ARL'XTRA diffractometer equipped with a Cu anode and a Si(Li) solid detector. The vertical θ : θ goniometer supports two Soller slits. A VTI RH 200 Relative Humidity generator device coupled to an Anton Paar HTK 1200R chamber allowed us to work with varying relative humidities. Experimental measurement parameters were 10 s counting time per 0.05 $^\circ$ 2 θ step. The divergence, the incident beam scatter, the diffracted beam scatter and the receiving slits were 1.00, 1.50, 0.45 and 0.30 mm wide, respectively. For XRD analysis we used 30–60 mg

of powdered samples. Data collection was performed at 303 K and 50% relative humidity (RH) after establishing an equilibrium period of 1 hour prior to each measurement.

The thermal gravimetric analyses (TGA) were recorded with a SETARAM TGA 92 microanalyser, from 293 to 1273 K with a heating rate of 5°mn^{-1} . Between 30 and 50 mg of sample were used for each measurement. All samples were held at the same relative humidity before the measurements to allow comparison between the dehydration peaks values.

Nitrogen adsorption–desorption experiments were performed to obtain information on the specific surface area and pore size distribution of the samples. They were performed at 77 K using a NOVA Surface Analyser QUANTACHROME INSTRUMENTS. 35 mg of sample was outgassed at 383 K for 24 h under a residual pressure of 0.01 Pa. The data were recorded for relative vapour pressures from 0.05 to 0.99. The specific surface area was determined using the Brunauer–Emmet–Teller (BET) equation (Brunauer et al., 1938) based upon the cross-sectional area of nitrogen (0.163 nm^2) at 77 K (Sing et al., 1985). The presence of micropores in the sample was assessed using the t-plot method (de Boer et al., 1966). Pore size distributions were calculated using the NOVAWin software according to the BJH method (Barrett et al., 1951) and with the Density Functional Theory (DFT) method ([Evans et al., 1986] and [Ravikovitch et al., 1998]).

2.3. Percolation experiments

To simulate the real hydro-mechanical behaviour of an engineered clay barrier under pressure in the context of subsurface waste landfill, oedometer cells equipped with a separated injection system were developed in the laboratory (Jullien and Lecomte, 2000). The experimental working parameters were optimized ([Jullien et al., 2002] and [Pothier et al., 2003]) (Fig. 1). The oedometer cell, with a 40 mm diameter, was equipped with a piston for mechanical stress control. The axial displacements of the piston were measured with a dial indicator with a $0.5 \mu\text{m}$ precision. Porous sintered bronze plates surrounded by Teflon waterproof rings were used as top and bottom of the cell. The porous plates were covered with filter paper to prevent pore obstruction by the clay. Concerning solute injection, the syringe, made of inert materials, allowed applying a constant mechanical pressure to the solution with the piston. The syringe piston displacements, which can be related to the injected volume, were picked up from a dial indicator. Negligible strains of the syringe were obtained in the range of applied injection pressures (below 1 MPa). For each experiment, 10 g of raw clay powder were firstly gradually compacted up to 0.5 MPa, and then totally unloaded, in order to simulate the over-consolidation of engineered clay barriers. A 0.3 MPa mechanical stress was then applied at the bottom side of the clay sample, whereas deionised water was injected by the syringe into the compacted clay sample under the same constant pressure of 0.3 MPa, applied to the upper boundary. Water intake and axial strain variations were monitored during percolation experiments. The leachates expelled from the clay were regularly collected, weighted and analysed to determine the cation concentrations by atomic absorption spectrometry and the pH values were also measured.

3. Results and discussion

3.1. Chemical characterization

The FTIR spectrum of the clay mineral exchanged with ammonium was compared with the one of the $< 2 \mu\text{m}$ fraction of SWy-2 (Fig. 2). The spectrum of the starting clay mineral was in

accordance with the results of Madejová and Komadel (2001) and showed a band at 3627 cm^{-1} assigned to the O–H bond stretching vibration of the octahedral sheets. A broad band between 3200 and 3600 cm^{-1} was due to the $\nu_{\text{symmetrical}}$ and $\nu_{\text{asymmetrical}}$ O–H bond stretching vibrations of water. The bending band of water was observed at 1637 cm^{-1} . The bands due to the Si–O bonds stretching vibrations were in the 1180 – 950 cm^{-1} range. The three bands at 950 – 850 cm^{-1} were assigned to (Al,Al)–O–H bending vibration around 918 cm^{-1} , (Al,Fe)–O–H bending vibration near 883 cm^{-1} and (Al,Mg)–O–H bending vibration at 849 cm^{-1} (Vantelon et al., 2001). Quartz impurities were observed at 800 and 780 cm^{-1} .

The authors who worked on NH_4^+ -exchanged clay minerals mainly focused their studies on the characterization by infrared spectroscopy ([Chourabi and Fripiat, 1981], [Srasra et al., 1994], [Petit et al., 1998], [Aranda and Ruiz-Hitzky, 1999], [Petit et al., 1999], [Bishop et al., 2002], [Pironon et al., 2003] and [Petit et al., 2006]). The stretching band of the O–H group bound to octahedral cations is located around 3630 cm^{-1} and our spectrum showed a sharp peak at 3627 cm^{-1} . The region of NH_4^+ stretching vibration (3300 – 2800 cm^{-1}) partially overlapped the OH stretching vibration bands of water (Fig. 2). In this region, Aranda and Ruiz-Hitzky (1999) deconvoluted the infrared spectrum of a NH_4^+ -exchanged Upton montmorillonite. They identified two OH stretching bands at 3532 cm^{-1} (asymmetric ν_{OH}) and 3435 cm^{-1} (symetric ν_{OH}) and three stretching bands attributed to NH vibrations at 3288 cm^{-1} , 3200 cm^{-1} and 3053 cm^{-1} . An unassigned band was also found at 2844 cm^{-1} . In our study, we mainly observed the stretching bands at 3270 cm^{-1} and 3080 cm^{-1} and another band at 2847 cm^{-1} (unassigned). Between 1700 and 700 cm^{-1} , the NH_4^+ bending vibration was found at 1427 cm^{-1} consistent with the results obtained by (Pironon et al., 2003), (Petit et al., 1998) and (Petit et al., 1999).

In our NH_4 -SWy-2 infrared spectrum (Fig. 2b), the infrared absorbance at wave number values between the OH band (3627 cm^{-1}) and the NH band (3270 cm^{-1}) had a low intensity very close to the supposed background intensity. This was not the case for the hydrated starting material (Fig. 2a) and our NH_4 -exchanged sample was a practically dehydrated montmorillonite where the ammonium ions replaced the interlayer cations. This assumption was confirmed by the results of Pironon et al. (2003) who showed that the bending band (1427 cm^{-1}) shifted towards high wave numbers with water pressure increase. During this experiment, they also observed an intensity increase of the water bending band at 1635 cm^{-1} . The NH_4 bending band wave number values were respectively 1425 cm^{-1} and 1450.2 cm^{-1} for a completely dehydrated sample and a totally hydrated one (Pironon et al., 2003). Our 1427 cm^{-1} value was close to the value observed by Pironon et al. (2003) for a dehydrated NH_4 -smectite; moreover, the water bending band intensity at 1635 cm^{-1} was low.

To conclude, the FTIR spectrum was in accordance with the results of several authors and showed that our NH_4 -exchanged smectite is nearly dehydrated.

The derivative of the TG curve (DTG, Fig. 3) which gives the mass loss showed several peaks assigned to the loss of adsorbed water, organic molecules and water evolved from hydroxyl groups. The dehydration peak maxima were approximately at the same temperature (359 K and 353 K for the original- and NH_4 -smectite respectively) but their intensities were different as a NH_4 -smectite is less hydrated than the original smectite which corroborates the FTIR results. The weak band at 600 K in the NH_4 -smectite curve (Fig. 3) corresponded to the thermal decomposition of NH_4^+ which was followed by the release of ammonia and the formation of H-montmorillonite ($\text{NH}_4^+ \rightarrow \text{NH}_3 + \text{H}^+$). This was in accordance with Yariv

(1985) which identified the peak related to ammonium decomposition at 603 K in a natural Wyoming bentonite. The temperature of the maximum of the endothermic peak assigned to the dehydroxylation shifted to a lower temperature after exchange (943 K for original smectite sample compared to 878 K for the NH_4 -smectite).

3.2. Mineralogical characterization and hydric behaviour

The XRD diagrams obtained at 303 K and 50% RH (Fig. 4) showed the classical patterns of smectites. The original smectite was widely studied in the literature, particularly by Chipera and Bish (2001) who assigned the pattern to 95% of smectite phase and 5% of impurities. The main impurity was quartz indicated by a significant peak at 0.334 nm (Fig. 4a). Quartz was also identified in the NH_4 -smectite (Fig. 4b).

The characteristic basal distance d_{001} was 1.45 nm for the original smectite and decreased to 1.19 nm after ammonium exchange. The broadened 001 reflections corresponded to heterogeneous systems where hydrated layers coexist with collapsed ones (Faisandier et al., 1998).

To characterize the crystalline swelling of the NH_4 -smectite, the variation of the basal spacing as a function of the relative water pressure was studied (Fig. 5) and compared with that of Na-smectite which is known to have a high crystalline swelling capacity (Norrish, 1954). In dehydrated state ($P/P_0 \cong 0$) the basal spacing was very close to 1.0 nm for both samples. For the Na-smectite sample the basal spacing increased slightly to 1.2 nm ($P/P_0 = 0.4$) with the beginning of hydration, which corresponds to water monolayers. In such states, the hydration of sodium ions allows the gradual opening of the interlayer spaces. For a relative pressure between 0.6 and 0.7, the basal spacing of the Na-smectite largely increased and reached values around 1.51–1.55 nm corresponding to water bilayers. The basal spacing of NH_4 -smectite remained relatively constant at around 1.20 nm from 0.15 to 0.9 P/P_0 , then it increased to 1.26 nm. Thus the hydration of the NH_4 -smectite was limited to one water layer. These results are in accordance with a study of Pironon et al. (2003) who observed that larger basal spacing were not reached at relative water pressures of 0.3–0.75.

The behaviour of both forms of the smectite can be interpreted from an argument based on the ionic radius. The ionic radius of NH_4^+ is between 0.136 nm (Aranda and Ruiz-Hitzky, 1999) and 0.143 nm (Pironon et al., 2003). This radius is close to the radius of K^+ and Rb^+ ions (Shannon, 1976). The Na^+ ionic radius (0.099 nm, Shannon, 1976) allows the collapse of the layers. However, the NH_4^+ ions which are larger than the cavity dimensions impede the complete closure of interlayer space. The swelling of interlayer space which begins almost simultaneously with the hydration of external surfaces is somewhat faster for the NH_4 -smectite. This is observed by a faster increase of the basal spacing at relative humidities below 15% faster with NH_4 -smectite than with Na-smectite (Fig. 5). Because of the higher hydration energy of the sodium ions, sodium smectite forms two interlamellar water layers at $P/P_0 > 0.75$ whereas only one interlamellar water layer is formed by the ammonium smectite. Diaz Pinthier (1999) showed that the NH_4^+ ion can establish several hydrogen bonds with oxygen atoms from the surface of the clay mineral layers. Formation of such hydrogen bonds may also limit the swelling of the interlayer space during hydration.

3.3. Specific surface area and pore size distribution

The adsorption–desorption curves (Fig. 6) revealed the classical features observed for swelling clays ([Michot and Villieras, 2002], [Neaman et al., 2003], [Marrocchi et al., 2005], [Perronnet et al., 2007] and [Le Forestier et al., 2010]), with the presence of both microporosity and mesoporosity. The adsorption isotherms were of type II, using the classification of IUPAC, with a hysteresis loop, corresponding to the capillary condensation of liquid nitrogen in mesopores (Sing et al., 1985). More precisely, the low pressure region ($P/P_0 < 0.42$) corresponds to the filling of micropores, the completion of the first monolayer on external particle faces, following by the beginning of the multilayer adsorption. In the high relative region ($P/P_0 > 0.42$), corresponding to the filling of the mesopores, the shape of the hysteresis loop is typical of type H3 with any limiting adsorption at high P/P_0 , which was observed with aggregates of plate-like particles giving rise to slit-shaped pores (Sing et al., 1985). The vertical closure of the hysteresis loop around 0.45 in P/P_0 is generally observed for such materials and is typical of closed mesoporosity inside clay aggregates (Neaman et al., 2003).

The BET and t-plot calculations applied to the nitrogen adsorption isotherm gave a total specific area of 31 and 35 $\text{m}^2 \text{g}^{-1}$ for original smectite. These values were twice lower than these of NH_4 -smectite (72 and 77 $\text{m}^2 \text{g}^{-1}$). BET specific surface areas are slightly lower than those derived from the t-plot calculation, which is in agreement with the fact that both samples appear slightly microporous. The specific surface areas of micropores were 10 $\text{m}^2 \text{g}^{-1}$ for original smectite and 22 $\text{m}^2 \text{g}^{-1}$ for NH_4 -smectite. They were in the same ratio as for mesopores (25 $\text{m}^2 \text{g}^{-1}$ for original smectite and 55 $\text{m}^2 \text{g}^{-1}$ for NH_4 -smectite). The results obtained with the original smectite (Na^+ , Ca^{2+} and K^+ as interlayer cations) and the NH_4 -smectite were in agreement with the studies of Bérend et al. (1995) on Wyoming montmorillonite who showed that the specific surface area increases with the ionic radii of the interlayer cations.

Different sizes of pores, such as micropores ($< 2 \text{ nm}$), mesopores (2–50 nm) and macropores ($> 50 \text{ nm}$) (Gregg and Sing, 1982), must be considered to describe the porosity of smectites. Mesopore size distributions were calculated according to the classical macroscopic BJH method (Barrett et al., 1951) and with the DFT method ([Evans et al., 1986] and [Ravikovitch et al., 1998]) for cylindrical pores. The BJH method leads generally to an underestimation of the pore sizes. The DFT simulation method is more realistic for micropores and narrow mesopores and was largely applied to the calculation of the pore size distribution (PSD) of clays ([Olivier and Occelli, 2001], [Occelli et al., 2002], [Gil and Gandía, 2003] and [Yang et al., 2006]). The same volume of adsorbed nitrogen corresponded to a lower P/P_0 of the desorption branch resulting indicating a lower free energy state. Thus, the desorption isotherm is closer to the true thermodynamic stability and the corresponding curve is generally used for the PSD determination. The results of the BJH and DFT calculations are shown in Fig. 7. The PSD is centred on only one value, approximately identical for both samples, but different for the two methods. The BJH calculations gave approximately 1.9 nm and DFT simulation led to a PSD centred at 2.6–2.7 nm after the NH_4^+ exchange, the width at half maximum of the PSD was smaller than for the original smectite one indicating a better homogeneity in pore size dimensions of the NH_4 -smectite.

Then, with a twice higher specific surface area of pores and an identical pore size, the NH_4 -smectite had a higher porosity than the original smectite one.

3.4. Hydro-mechanical behaviour

The measured injected volume as a function of time displayed a constant water flow in both percolation experiments (original smectite and NH_4 -smectite) after hundred hours, which corresponded to the end of the transient hydraulic state (Fig. 8). This constant injected flow allowed to calculate the hydraulic conductivity, k (m s^{-1}), from the Darcy's law, using the expression elaborated for a saturated medium (Domenico and Schwartz, 1990): $k = Q/i S$, where Q is the injected flow ($\text{m}^3 \text{s}^{-1}$) at the steady state, i the hydraulic gradient and S the cross-sectional area of the oedometer (m^2). The hydraulic conductivity calculations yielded values of $0.3 \cdot 10^{-12}$ and $1.4 \cdot 10^{-12} \text{ m s}^{-1}$, for the original smectite and the NH_4 -smectite, respectively. The ammonium-exchanged montmorillonite is almost five times more permeable than the starting one. This hydraulic conductivity of NH_4 -smectite is in the same magnitude than Fo-Ca bentonite ($k = 1.1 \cdot 10^{-12} \text{ m s}^{-1}$), compacted and soaked with water under the same experimental conditions (Jullien et al., 2002). Andrejkovičová et al. (2008) obtained permeability coefficients on the order of $10^{-11} \text{ m s}^{-1}$ with bentonite from the Slovakia deposit.

The axial displacements of the piston measured during the percolation experiments with water allow to derive the axial swelling strain ε_1 (Fig. 9). The axial deformation of the original smectite increased very quickly in the first minutes, with a value of 1% after one hour. However, the ammonium-exchanged smectite revealed no axial deformation for the first 12 h. The permanent mechanical regime defined by strain equilibrium (Jullien et al., 2002) was reached after 150 h of water percolation for NH_4 -smectite, with an asymptotic value of 2.2%, while the original smectite was still swelling. The permanent mechanical regime of the original smectite was effective after 100 days of percolation (Fig. 9a), which pointed out the slow kinetics of macroscopic swelling. The original smectite, which mainly contains sodium and calcium ions, was easily hydrated and had a significant swelling capacity, with a value of 10%. In comparison, the sodium-exchanged Wyoming smectite (Na-SWy-2) showed a higher swelling strain at equilibrium with a value of 37%, obtained with the same protocol and an equivalent oedometer cell (Le Forestier et al., 2010). The macroscopic swelling is obviously linked to the nature of the interlayer cation.

During the percolation experiment with the original smectite, the pH value of leachates increased up to 9 because of the release of some sodium and calcium cations (Fig. 10). Around 8 meq/100 g of the interlayer cations (Ca^{2+} , K^+ and mainly Na^+) were released into the solution at the end of the percolation experiment of the original smectite. On the contrary, the pH value slightly decreased with NH_4 -smectite (pH = 7.2). In this case, no Ca^{2+} , K^+ and Na^+ ions were detected in solutions, as expected (NH_4^+ concentrations were not analysed in the leachates). Despite these small trends, the compositions of both smectites remained almost constant after percolation (Table 1). The XRD patterns did not differ before and after the experiment (Fig. 11). The basal spacing remained constant at 1.19 nm for the NH_4 -smectite. The same feature was observed for the original smectite with d_{001} constant and equal to 1.32 nm. Compaction and percolation of water through the NH_4 -smectite did not change the distribution of water molecules in the interlayer space.

By considering axial deformation and hydraulic conductivity, it can be concluded that the reduced swelling of the NH_4 -smectite limited the impermeability. The macroscopic swelling is the combined result of the interlayer hydration of the exchangeable cations, the interparticular swelling connected to the diffuse double layer and the formation or

delamination of particles ([Laird, 2006](#)). Because of the limited interlayer hydration of ammonium smectite with the increase of the water pressure, the macroscopic swelling observed for NH₄-smectite was lower than for original smectite. The specific surface area of NH₄-smectite was twice that of the original smectite, supposing a disaggregation and possibly some delamination of the particles which favoured the water transfer and increased the hydraulic conductivity.

4. Conclusion

A very high quantity of ammonium ions in the leachate was reported by several authors so that it was necessary to investigate the behaviour of a NH₄-smectite in waste landfill conditions to predict the changes which can occur at the bottom of these landfills.

A combined study using FTIR spectroscopy, thermal analysis and X-ray diffraction showed that the hydration capacity of NH₄-smectite was lower than that of the original smectite. With increasing hydration, the basal spacing remained constant indicating the one-layer water hydration. The hydro-mechanical changes of the engineered barrier in a waste landfill were tested by percolation experiments. Even if the permeability remained at acceptable levels with a hydraulic conductivity $< 10^{-9} \text{ m s}^{-1}$, it significantly increased after the ammonium exchange. The result was in agreement with the increase of the specific surface area. Moreover, the macroscopic swelling of the barrier decreased.

This study shows the negative impact of the exchange of the interlayer cations of smectites by NH₄⁺ ions from leachates, particularly in terms of permeability. The environmental consequences can be hazardous for the long term. A monitoring of the site is therefore necessary for many years, particularly considering the type of soil and analyses of the nearby groundwater.

Acknowledgments

The authors are grateful to the editor Gerhard Lagaly and the two anonymous referees for reviewing the manuscript and for their valuable comments on the paper. The authors also gratefully thank Marielle Hatton and Patrick Baillif for their technical assistance and Patrick Lecomte for the conception of the oedometer cell.

References

- [Alawaji, 1999](#) H.A. Alawaji, Swell and compressibility characteristics of sand–bentonite mixtures inundated with liquids, *Applied Clay Science* **15** (1999), pp. 411–430
- [Andrejkovičová et al., 2008](#) S. Andrejkovičová, I. Janotka and P. Komadel, Evaluation of geotechnical properties of bentonite from Lieskovec deposit, Slovakia, *Applied Clay Science* **38** (2008), pp. 297–303.

Aranda and Ruiz-Hitzky, 1999 P. Aranda and E. Ruiz-Hitzky, Poly(ethylene oxide)/NH₄⁺-smectite nanocomposites, *Applied Clay Science* **15** (1999), pp. 119–135.

Barrett et al., 1951 E.P. Barrett, L.G. Joyner and P.P. Halenda, The determination of pore volume and area distributions in porous substances. I. Computations from nitrogen isotherms, *Journal of the American Chemical Society* **73** (1951), pp. 373–380.

Baun and Christensen, 2004 D. Baun and T. Christensen, Speciation of heavy metals in landfill leachate: a review, *Waste Management & Research* **23** (2004), pp. 3–23

Belevi and Baccini, 1989 H. Belevi and P. Baccini, Long-term behavior of municipal solid waste landfills, *Waste Management & Research* **7** (1989), pp. 43–56

Bérend et al., 1995 I. Bérend, J.M. Cases, M. François, J.P. Uriot, L. Michot, A. Masion and F. Thomas, Mechanism of adsorption and desorption of water vapor by homoionic montmorillonites: 2. The Li⁺, Na⁺, K⁺, Rb⁺ and Cs⁺-exchanged forms, *Clays and Clay Minerals* **43** (1995), pp. 324–336.

Bishop et al., 2002 J.L. Bishop, A. Banin, R.L. Mancinelli and M.R. Klovstad, Detection of soluble and fixed NH₄⁺ in clay minerals by DTA and IR reflectance spectroscopy: a potential tool for planetary surface exploration, *Planetary and Space Science* **50** (2002), pp. 11–19.

Brunauer et al., 1938 S. Brunauer, P.H. Emmett and E. Teller, Adsorption of gases in multimolecular layers, *Journal of the American Chemical Society* **60** (1938), pp. 309–319.

Chipera and Bish, 2001 S.J. Chipera and D.L. Bish, Baseline studies of the Clay Minerals Society Source Clays: powder X-ray diffraction analyses, *Clays and Clay Minerals* **49** (2001), pp. 398–409.

Chourabi and Fripiat, 1981 B. Chourabi and J.J. Fripiat, Determination of tetrahedral substitutions and interlayer surface heterogeneity from vibrational spectra of ammonium in smectites, *Clays and Clay Minerals* **29** (1981), pp. 260–268.

Christensen et al., 2001 T.H. Christensen, P. Kjeldsen, P.L. Bjerg, D.L. Jensen, J.B. Christensen, A. Baun, H.-J. Albrechtsen and G. Heron, Biogeochemistry of landfill leachate plumes, *Applied Geochemistry* **16** (2001), pp. 659–718.

Coméaga, 1997 Coméaga, L., 1997. Dispositifs d'étanchéité par géosynthétiques bentonitiques dans les centres de stockage de déchets. Ph. D. Thesis, I.N.S.A. Lyon, France.

Daniel et al., 1993 D.E. Daniel, H.Y. Shan and J.D. Anderson, Effects of partial wetting on the performance of the bentonite component of a geosynthetic clay liner, *Proceedings Geosynthetics'93 Vol. 3*, Publication of the Industrial Fabrics Association International, Saint Paul, Minnesota, United States of America (1993), pp. 1483–1496.

de Boer et al., 1966 J.H. de Boer, B.C. Lippens, B.G. Linsen, J.C.P. Broekhoff, A. van den Heuvel and T.J. Osinga, The t-curve of multimolecular N₂ adsorption, *Journal of Colloid and Interface Science* **21** (1966), pp. 405–414.

Diaz Pinthier, 1999 Diaz Pinthier, M., 1999. Etude des interactions cations compensateurs/feuilletés dans les argiles: contribution à la connaissance des mécanismes de rétention sélective. Ph. D. Thesis, Orléans University, France.

Dockhorn et al., 1997 T. Dockhorn, L. Chang and N. Dichtl, Removal of nitrogen from landfill leachate by using SBR-Technology, *Proceedings of the Sixth International Landfill Symposium, Sardinia '97 Vol. II*, CISA Publisher, Cagliari, Italy (1997), pp. 303–314.

Domenico and Schwartz, 1990 P.A. Domenico and F.W. Schwartz, Physical and Chemical Hydrogeology, Wiley, New York, United States of America (1990).

Egloffstein, 2001 T.A. Egloffstein, Natural bentonites-influence of the ion exchange and partial desiccation on permeability and self-healing capacity of bentonites used in GCLs, *Geotextiles and Geomembranes* **19** (2001), pp. 427–444.

Ehrig, 1989 H.J. Ehrig, Leachate quality. In: T.H. Christensen, R. Cossu and R. Stegmann, Editors, *Sanitary Landfilling: Process, Technology and Environmental Impact*, Academic Press, London, United Kingdom (1989), pp. 213–230.

Evans et al., 1986 R. Evans, U. Marini Bettolo Marconi and P. Tarazona, Capillary condensation and adsorption in cylindrical and slit-like pores, *Journal of the Chemical Society, Faraday Transactions 2: Molecular and Chemical Physics* **82** (1986), pp. 1763–1787.

Faisandier et al., 1998 K. Faisandier, C.H. Pons, D. Tchoubar and F. Thomas, Structural organization of Na- and K-montmorillonite suspensions in response to osmotic and thermal stresses, *Clays and Clay Minerals* **46** (1998), pp. 636–648.

Gaucher et al., 2006 E.C. Gaucher, D. Guyonnet and D. Cazaux, Confinement des déchets: les apports de la géochimie pour la compréhension des barrières argileuses, *Environment & Technique* **256** (2006), pp. 29–33.

Gautier et al., 2009 M. Gautier, F. Muller, J.-M. Béný, L. Le Forestier, P. Albéric and P. Baillif, Interactions of ammonium smectite with low-molecular-weight carboxylic acids, *Clay Minerals* **44** (2009), pp. 207–219.

Gil and Gandía, 2003 A. Gil and L.M. Gandía, Microstructure and quantitative estimation of the micropore-size distribution of an alumina-pillared clay from nitrogen adsorption at 77K and carbon dioxide adsorption at 273K, *Chemical Engineering Science* **58** (2003), pp. 3059–3075.

Gregg and Sing, 1982 S.J. Gregg and K.S.W. Sing, Adsorption, Surface Area and Porosity (Second edition), Academic Press, London, United Kingdom (1982).

Guyonnet et al., 2005 D. Guyonnet, E. Gaucher, H. Gaboriau, C.-H. Pons, C. Clinard, V. Norotte and G. Didier, Geosynthetic clay liner interaction with leachate: correlation between permeability, microstructure, and surface chemistry, *Journal of Geotechnical and Geoenvironmental Engineering* **131** (2005), pp. 740–749.

Jullien and Lecomte, 2000 Jullien, A., Lecomte, P., 2000. Dispositif perméamétrique à injecteur à pression contrôlée séparé. Brevet Français N°00/07820.

Jullien et al., 2002 A. Jullien, C. Proust, L. Le Forestier and P. Baillif, Hydro-chemio-mechanical coupling effects on permeability and swelling behaviour of a Ca smectite soaked by Cu solutions, *Applied Clay Science* **21** (2002), pp. 143–153.

Kjeldsen et al., 2002 P. Kjeldsen, M.A. Barlaz, A.P. Rooker, A. Baun, A. Ledin and T.H. Christensen, Present and long-term composition of MSW landfill leachate: A review, *Critical Reviews in Environmental Science and Technology* **32** (2002), pp. 297–336.

Kruempelbeck and Ehrig, 1999 I. Kruempelbeck and H.-J. Ehrig, Long-term behaviour of municipal solid waste landfills in Germany, *Proceedings of the Seventh International Waste Management and Landfill Symposium, Sardinia'99*, CISA Publisher, Environmental Sanitary Engineering Centre, Cagliari, Italy (1999), pp. 27–36 I.

Laird, 2006 D.A. Laird, Influence of layer charge on swelling of smectites, *Applied Clay Science* **34** (2006), pp. 74–87.

Le Forestier et al., 2010 L. Le Forestier, F. Muller, F. Villiéras and M. Pelletier, Textural and hydration properties of a synthetic montmorillonite compared with a natural Na-exchanged clay analogue, *Applied Clay Science* **48** (2010), pp. 18–25

Lin, 1998 Lin, L., 1998. Effect of wet–dry cycling on swelling and hydraulic conductivity of geosynthetic clay liners. Master Thesis, University of Wisconsin-Madison, United States of America.

Madejová and Komadel, 2001 J. Madejová and P. Komadel, Baseline studies of the Clay Minerals Society source clays: infrared methods, *Clays and Clay Minerals* **49** (2001), pp. 410–432.

Malfoy, 2003 Malfoy, C., 2003. Influence du cation échangeable et des hétérogénéités minérales sur le comportement rhéologique de suspensions de smectite. Ph. D. Thesis, Poitiers University, France.

Marrocchi et al., 2005 Y. Marrocchi, A. Razafitianamaharavo, L.J. Michot and B. Marty, Low-pressure adsorption of Ar, Kr, and Xe on carbonaceous materials (kerogen and carbon blacks), ferrihydrite, and montmorillonite: Implications for the trapping of noble gases onto meteoritic matter, *Geochimica et Cosmochimica Acta* **69** (2005), pp. 2419–2430.

McBride, 1994 M.B. McBride, *Environmental Chemistry of Soils*, Oxford University Press, New York, United States of America (1994).

Michot and Villiéras, 2002 L.J. Michot and F. Villiéras, Assessment of surface energetic heterogeneity of synthetic Na-saponites. The role of layer charge, *Clay Minerals* **37** (2002), pp. 39–57.

Mohan et al., 1999 K.K. Mohan, M.G. Reed and H.S. Fogler, Formation damage in smectitic sandstones by high ionic strength brines, *Colloids and Surfaces A: Physicochemical and Engineering Aspects* **154** (1999), pp. 249–257.

Neaman et al., 2003 A. Neaman, M. Pelletier and F. Villieras, The effects of exchanged cation, compression, heating and hydration on textural properties of bulk bentonite and its corresponding purified montmorillonite, *Applied Clay Science* **22** (2003), pp. 153–168.

Norrish, 1954 K. Norrish, The swelling of montmorillonite, *Discussions of the Faraday Society* **18** (1954), pp. 120–134.

Occelli et al., 2002 M.L. Ocelli, J.P. Olivier, J.A. Perdigon-Melon and A. Auroux, Surface area, pore volume distribution, and acidity in mesoporous expanded clay catalysts from hybrid density functional theory (DFT) and adsorption microcalorimetry methods, *Langmuir* **18** (2002), pp. 9816–9823.

Olivier and Ocelli, 2001 J.P. Olivier and M.L. Ocelli, Surface area and microporosity of a pillared interlayered clay (PILC) from a hybrid density functional theory (DFT) method, *The Journal of Physical Chemistry B* **105** (2001), pp. 623–629.

Öman and Junestedt, 2008 C.B. Öman and C. Junestedt, Chemical characterization of landfill leachates-400 parameters and compounds, *Waste Management* **28** (2008), pp. 1876–1891.

Pelletier et al., 1999 M. Pelletier, L.J. Michot, O. Barrès, B. Humbert, S. Petit and J.-L. Robert, Influence of KBr conditioning on the infrared hydroxyl-stretching region of saponites, *Clay Minerals* **34** (1999), pp. 439–445.

Perronnet et al., 2007 M. Perronnet, F. Villiéras, M. Jullien, A. Razafitianamaharavo, J. Raynal and D. Bonnin, Towards a link between the energetic heterogeneities of the edge faces of smectites and their stability in the context of metallic corrosion, *Geochimica et Cosmochimica Acta* **71** (2007), pp. 1463–1479.

Petit et al., 1998 S. Petit, D. Righi, J. Madejová and A. Decarreau, Layer charge estimation of smectites using infrared spectroscopy, *Clay Minerals* **33** (1998), pp. 579–591.

Petit et al., 1999 S. Petit, D. Righi, J. Madejová and A. Decarreau, Interpretation of the infrared NH_4^+ spectrum of the NH_4^+ -clays: application to the evaluation of the layer charge, *Clay Minerals* **34** (1999), pp. 543–549.

Petit et al., 2006 S. Petit, D. Righi and J. Madejová, Infrared spectroscopy of NH_4^+ -bearing and saturated clay minerals: a review of the study of layer charge, *Applied Clay Science* **34** (2006), pp. 22–30.

Pironon et al., 2003 J. Pironon, M. Pelletier, P. de Donato and R. Mosser-Ruck, Characterization of smectite and illite by FTIR spectroscopy of interlayer NH_4^+ cations, *Clay Minerals* **38** (2003), pp. 201–211.

Pivato and Raga, 2006 A. Pivato and R. Raga, Tests for the evaluation of ammonium attenuation in MSW landfill leachate by adsorption into bentonite in a landfill liner, *Waste Management* **26** (2006), pp. 123–132.

Pothier et al., 2003 C. Pothier, A. Jullien, C. Proust and P. Lecomte, Etude des phénomènes de transfert de métaux lourds dans une smectite, *Revue Française de Géotechnique* **103** (2003), pp. 33–42.

Ravikovitch et al., 1998 P.I. Ravikovitch, G.L. Haller and A.V. Neimark, Density functional theory model for calculating pore size distributions: pore structure of nanoporous catalysts, *Advances in Colloid and Interface Science* **76–77** (1998), pp. 203–226.

Robinson and Luo, 1991 H.D. Robinson and M.M.H. Luo, Characterization and treatment of leachates from Hong Kong landfill sites, *Water and Environment Journal* **5** (1991), pp. 326–335.

Shackelford, 1994 C.D. Shackelford, Waste–soil interactions that alter hydraulic conductivity. In: D.D. Daniel and S.J. Trautwein, Editors, *Hydraulic Conductivity and Waste Contaminant Transport in Soil. ASTM STP 1142*, American Society for Testing and Materials, Philadelphia, United States of America (1994), pp. 111–168.

Shackelford et al., 2000 C.D. Shackelford, C.H. Benson, T. Katsumi, T.B. Edil and L. Lin, Evaluating the hydraulic conductivity of GCLs permeated with non-standard liquids, *Geotextiles and Geomembranes* **18** (2000), pp. 133–161.

Shannon, 1976 R.D. Shannon, Revised effective ionic radii and systematic studies of interatomic distances in halides and chalcogenides, *Acta Crystallographica Section A* **32** (1976), pp. 751–767.

Sing et al., 1985 K.S.W. Sing, D.H. Everett, R.A.W. Haul, L. Moscou, R.A. Pierotti, J. Rouqu  rol and T. Siemieniewska, Reporting physisorption data for gas/solid systems with special reference to the determination of surface area and porosity, *Pure & Applied Chemistry* **57** (1985), pp. 603–619   1985 IUPAC.

Srasra et al., 1994 E. Srasra, F. Bergaya and J.J. Fripiat, Infrared spectroscopy study of tetrahedral and octahedral substitutions in an interstratified illite–smectite clay, *Clays and Clay Minerals* **42** (1994), pp. 237–241.

Studds et al., 1996 P.G. Studds, D.I. Stewart and T.W. Cousens, The effect of ion valence on the swelling behavior of sodium bentonite, *Proceedings of the Fourth International Conference on Re-use of Contaminated Land and Landfills, Polluted and Marginal Land-96*, Engineering Technics Press, Edinburgh, United Kingdom (1996), pp. 139–142.

Stumm, 1992 W. Stumm, Chemistry of the Solid–Water Interface: Processes at the Mineral–Water and Particle–Water Interface in Natural Systems, John Wiley and Sons, New York, United States of America (1992).

Trabelsi et al., 2000 I. Trabelsi, H. Horibe, N. Tanaka and T. Matsuto, Origin of low carbon/nitrogen ratios in leachate from old municipal solid waste landfills, *Waste Management & Research* **18** (2000), pp. 224–234.

Vantelon et al., 2001 D. Vantelon, M. Pelletier, L.J. Michot, O. Barres and F. Thomas, Fe, Mg and Al distribution in the octahedral sheet of montmorillonites. An infrared study in the OH-bending region, *Clay Minerals* **36** (2001), pp. 369–379.

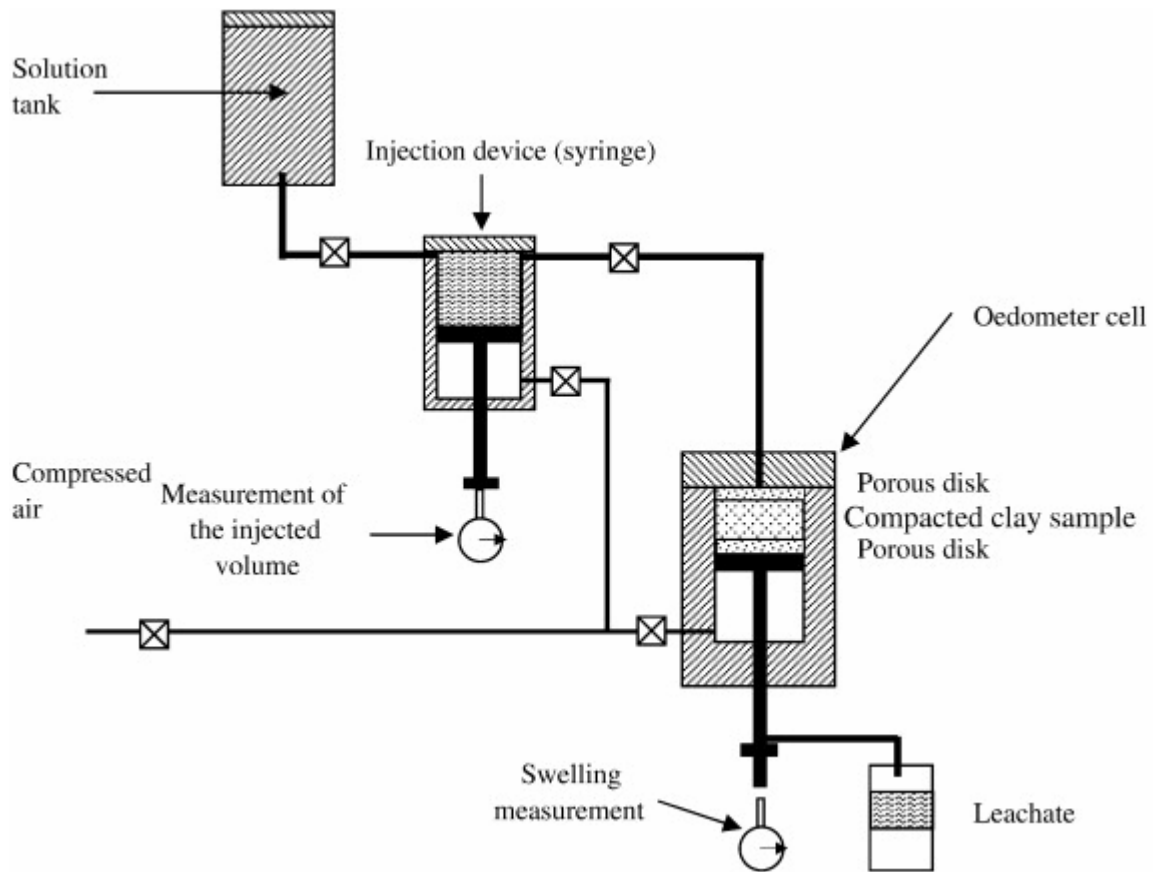
Yang et al., 2006 T. Yang, X.-D. Wen, J. Li and L. Yang, Theoretical and experimental investigations on the structures of purified clay and acid-activated clay, *Applied Surface Science* **252** (2006), pp. 6154–6161.

Yariv, 1985 S. Yariv, Study of the adsorption of organic molecules on clay minerals by differential thermal analysis, *Thermochimica Acta* **88** (1985), pp. 49–68.

Figures and tables

Table 1. Chemical composition reported in oxide mass contents of calcined samples measured by ICP-AES. The N content obtained by elemental N analysis is expressed in smectite ammonium oxide. The cationic exchange capacity CEC is expressed in meq/100 g of calcined smectite.

	SiO ₂	Al ₂ O ₃	Fe ₂ O ₃	MnO	MgO	TiO ₂	CaO	Na ₂ O	K ₂ O	(NH ₄) ₂ O	CEC
Original state											
Original smectite	67.65	22.06	4.61	0.01	2.80	0.11	1.06	1.50	0.20	0	83.3
NH ₄ -smectite	69.09	22.81	4.71	0.01	2.66	0.12	0.17	0.18	0.20	1.79	79.3
After water percolation											
Original smectite	68.06	20.53	4.15	0.13	2.94	0.15	2.02	1.34	0.69	0	u.
NH ₄ -smectite	67.23	22.69	4.85	0.02	2.75	0.12	0.38	0.09	0.18	1.70	u.



u: undetermined.

Fig. 1. Equipment of the oedometer cell (from Jullien et al., 2002).

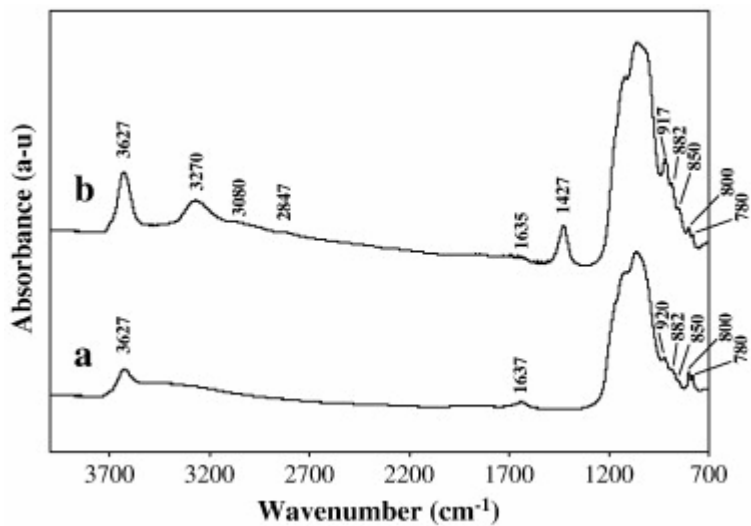


Fig. 2. Fourier transform infrared (FTIR) spectra of (a) untreated-smectite and (b) NH₄-smectite samples recorded at room temperature with the IR microscope.

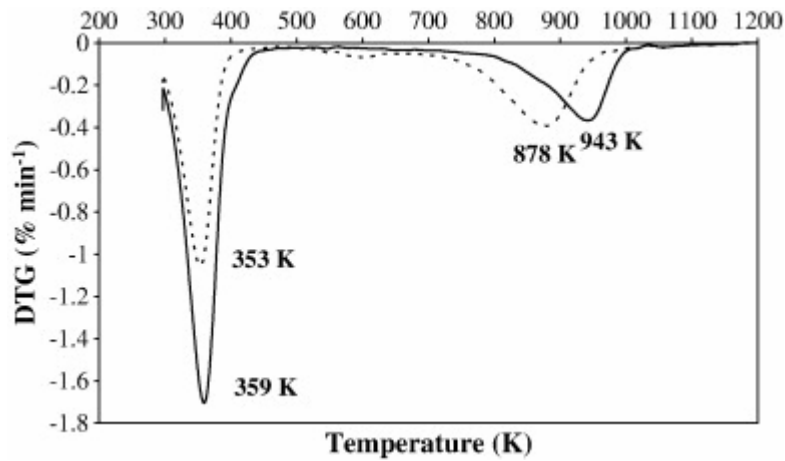


Fig. 3. Differential thermo gravimetric (DTG) curves of original smectite (plain line) and NH₄-smectite (dotted line).

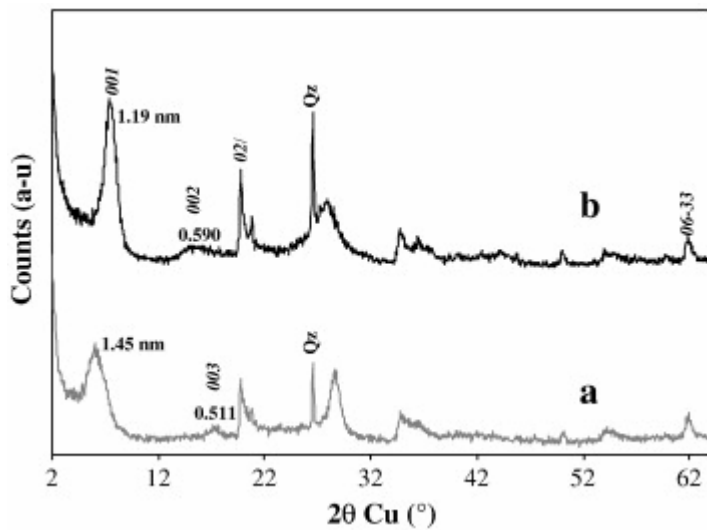


Fig. 4. X-ray diffraction patterns of (a) original smectite and (b) NH₄-smectite. Qz indicates quartz.

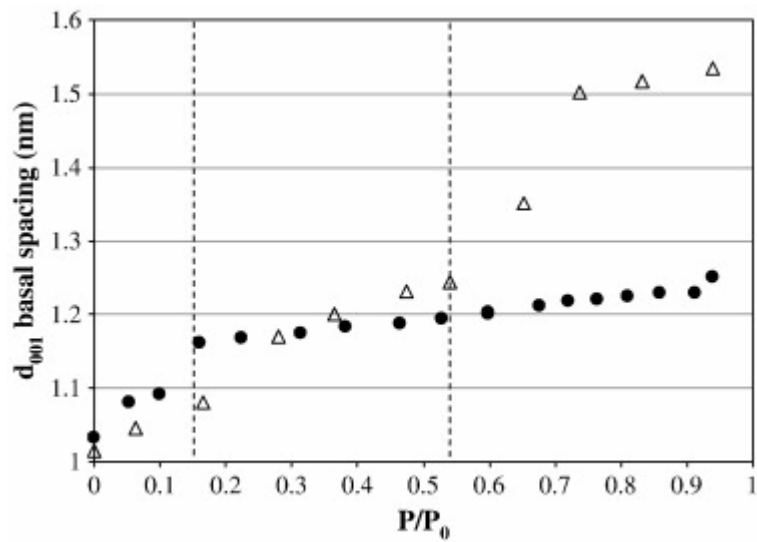


Fig. 5. Variation of the d_{001} versus the partial pressure of water for Na-smectite (open triangles) and NH_4 -smectite (black circles).

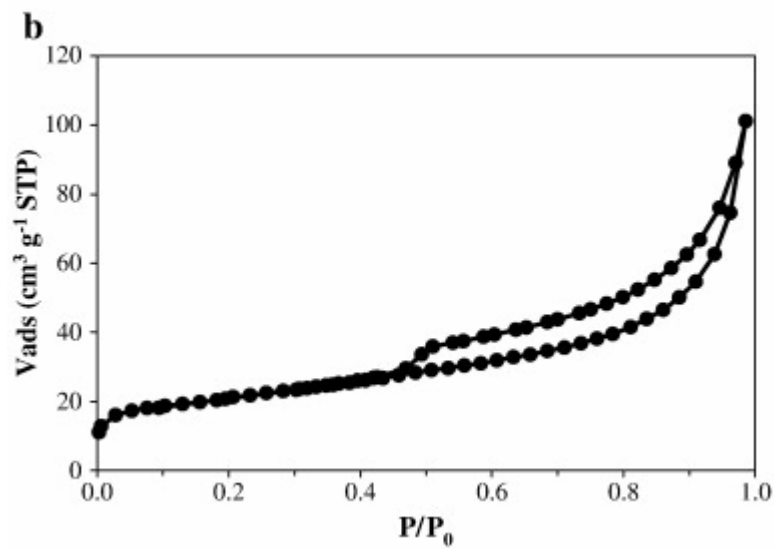
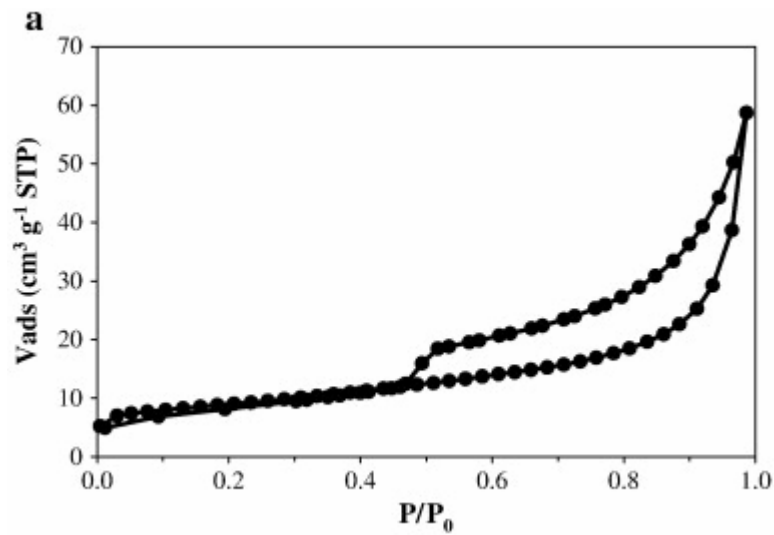


Fig. 6. Adsorption-desorption isotherms of nitrogen at 77 K for (a) original smectite and (b) NH₄-smectite.

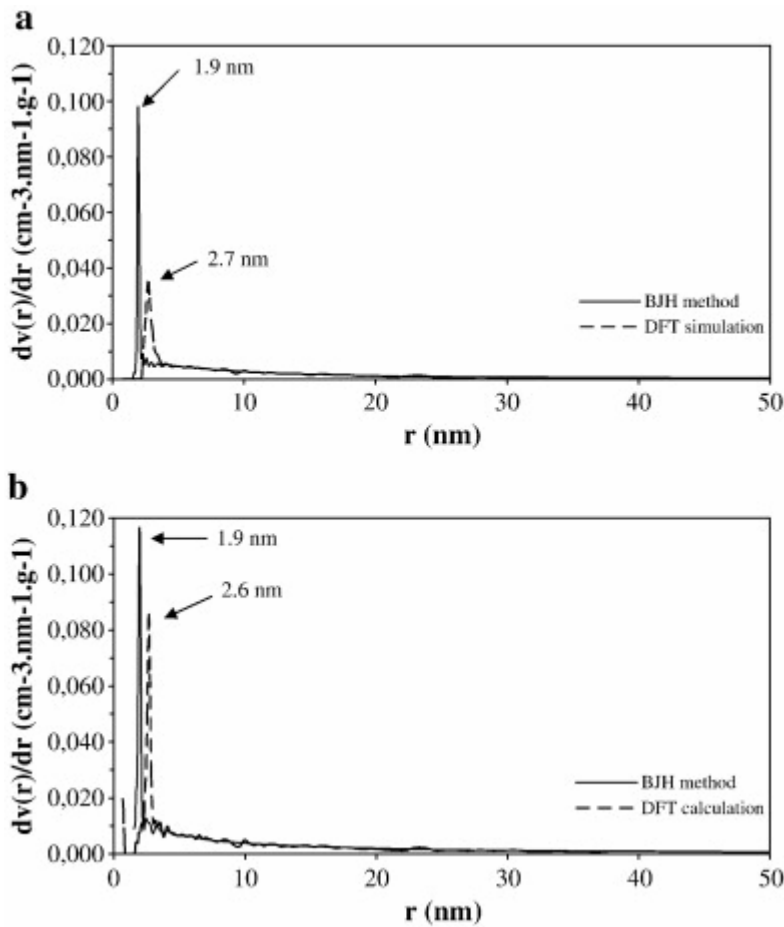


Fig. 7. Pore size distribution (PSD), calculated from nitrogen desorption isotherms (Fig. 6), (a) original smectite and (b) NH₄-smectite. Solid line, PSD obtained with BJH method; dotted line, PSD obtained with DFT simulation.

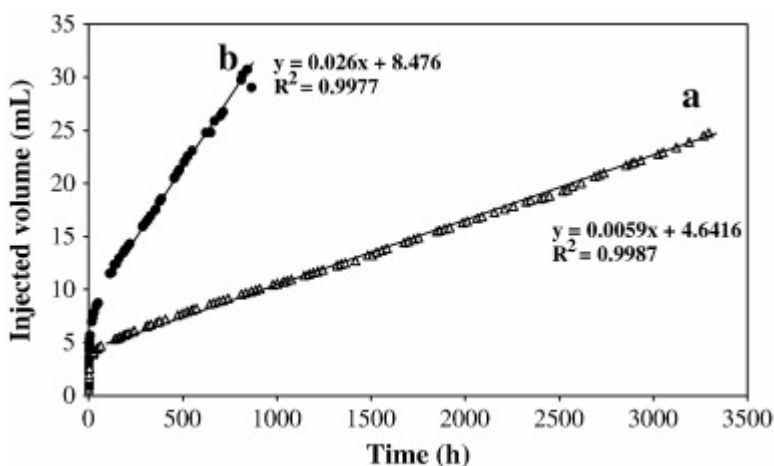


Fig. 8. Injected volume during percolation experiments of water in (a) original smectite (open triangles) and (b) NH₄-smectite (black circles).

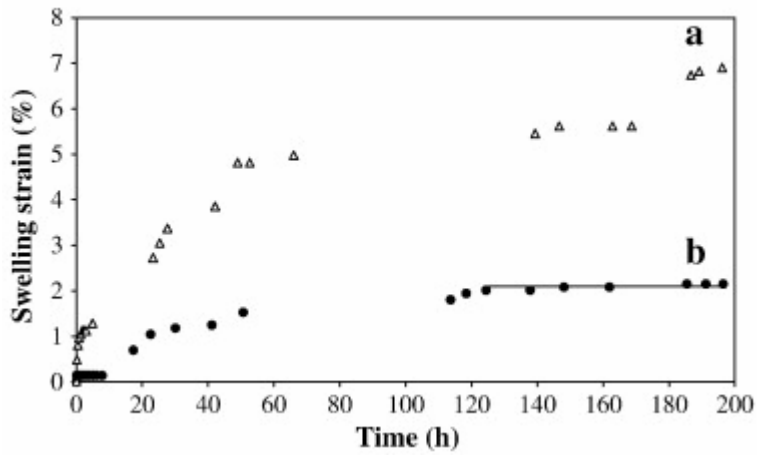
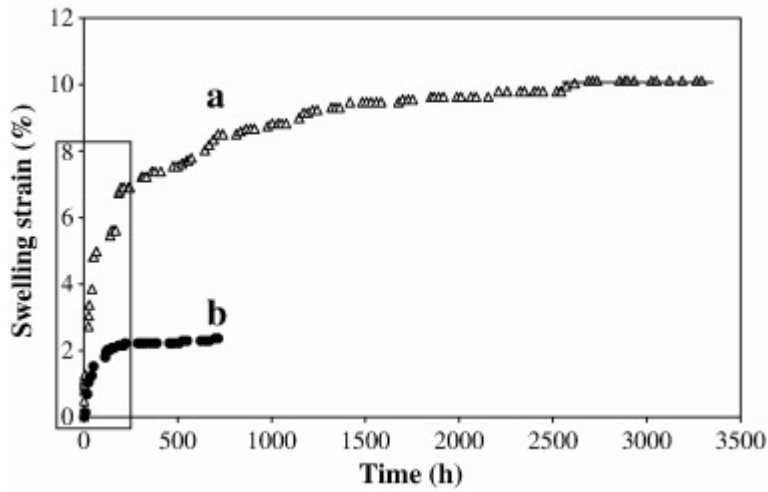


Fig. 9. Swelling strain during percolation experiments of water in (a) original smectite and (b) NH_4 -smectite. The graph below is a zoom of the 0-200 h range.

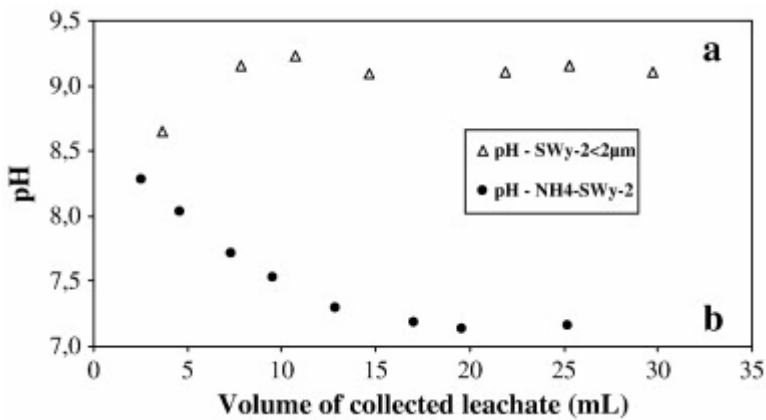


Fig. 10. pH as a function of leachate quantity from original smectite (a, open triangles) and NH_4 -smectite (b, black circle).

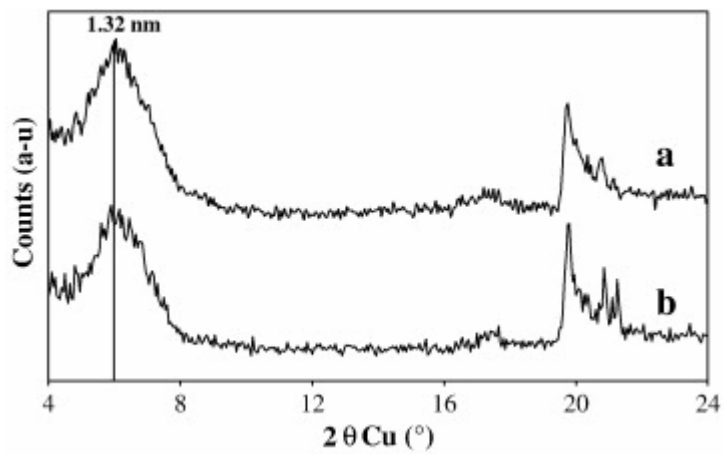


Fig. 11. X-ray diffraction patterns of NH_4 -smectite (a) before and (b) after the percolation experiments with water.